



Tracking deformation velocity via PSI and SBAS as a sign of landslide failure: an open-pit mine-induced landslide in Himmetoğlu (Bolu, NW Turkey)

Remzi Eker¹ · Abdurrahim Aydın² · Tolga Görüm³

Received: 7 February 2023 / Accepted: 28 February 2024
© The Author(s) 2024

Abstract

A destructive landslide occurred in Himmetoğlu village in Göynük District (Bolu, NW Turkey) caused by open-pit coal mining activities. Field observations after the landslide failure and interviews with villagers motivated us to question the possibility of using satellite SAR data to detect precursory signs of failure with regard to deformation velocity. In this study, first, landslide deformations were mapped by applying the digital elevation model (DEM) of Difference (DoD) method using DEMs from aerial photography and UAV data. However, the primary aim was to track deformation velocity as a sign of landslide failure with persistent scatterers interferometry (PSI) and small baseline subset (SBAS) methods from Sentinel-1A data. For the SBAS, the deformation velocity for ascending and descending orbits varied between -12 and 39 mm year⁻¹ and between -24 and 6 mm year⁻¹, respectively. For the PSI, the deformation velocity for ascending and descending orbits varied between -16 and 31 mm year⁻¹ and between -18 and 20 mm year⁻¹, respectively. PSI and SBAS resulted in sharply changing line-of-sight displacement rates, which were interpreted as slope failure signs, from three months prior to the landslide. In addition, higher deformation velocities were observed in locations closer to landslide crack as expected. Based on our findings, we concluded that SAR interferometric time-series analysis have the makings of being used as a suitable approach in early discerning and avoiding potential slope failures in open-pit mining areas, when it is made carefully by observing the progress in mining activities by considering the other factors such as rainfall and earthquakes.

Keywords Deformation velocity · DoD · InSAR · Landslide · Open-pit mining · UAV

✉ Remzi Eker
remzi.eker@ikc.edu.tr

¹ Faculty of Forestry, Department of Forest Engineering, İzmir Katip Çelebi University, Çiğli Main Campus, 35620 İzmir, Turkey

² Faculty of Forestry, Remote Sensing & GIS Laboratory, Konuralp Campus, Düzce University, 81620 Düzce, Turkey

³ Eurasia Institute of Earth Sciences, Istanbul Technical University, Istanbul, Turkey

1 Introduction

Landslides can be triggered by several natural and anthropogenic agents. Human activities such as urbanization, road construction, forest management practices, agricultural activities, and mining increase the likelihood of landslides resulting in many casualties and huge economic losses. For example, in mining areas, especially for open-pit mines, ground deformations and slope instabilities frequently generate major geological problems, both during mining operations and for many years after their closure (Herrera et al. 2010). Mining activities can significantly impact the geomorphology and hydrology of catchments by causing abrupt and extensive land-use changes that affect vegetation, soil, bedrock, and landforms (Martín-Duque et al. 2010; Sonter et al. 2014). Open-pit mining operations also cause ground deformations that lead to potential slope instabilities (Gourmelen et al. 2007). Surface mining activities, ore exploration, and stripping and dumping of the overburden cause changes in the land cover and land use in mine areas (Demirel et al. 2011). In this respect, the management of unstable slopes is a fundamental challenge with open-pit mines (Intrieri et al. 2019).

In the last decade, remote-sensing techniques have made remarkable advances in gathering terrain information, thus providing new opportunities for a better understanding of Earth surface processes (Tarolli 2014). The increase in the amount of available remote-sensing data has led to the evolution of novel techniques for mapping and monitoring unstable slopes (Friedl and Hölbling 2015). Multiple remote-sensing methods, including synthetic aperture radar (SAR), optical, light detection and ranging (LiDAR), orthophotography, and digital elevation models (DEMs) obtained from space-borne, airborne, and ground-based platforms can be utilized in studies of ground deformation and landslides (Zhao and Lu 2018). In particular, the mapping and monitoring of ground deformations at centimeter to millimeter resolution using space-borne SAR interferometry have reached a remarkable level of development over the last few decades (Wegmüller et al. 2010). InSAR time series are well-established radar techniques for the monitoring of earth deformations with millimeter accuracy. The precision of InSAR time-series techniques can reach up to 1 mm year^{-1} even it is not usual and common precision that only can be reached in particular scenarios (Aobpaet et al. 2013). Various interferometric synthetic aperture radar (InSAR) techniques have gained importance in ground deformation (subsidence and uplifting) studies. These include both traditional differential InSAR and advanced interferometric time series, such as the persistent scatterer interferometry (PSI) and small baseline subset (SBAS) (Aly et al. 2009; Zhao et al. 2009; Prati et al. 2010; Osmanoglu et al. 2011; Canova et al. 2012; Aobpaet et al. 2013; Chen et al. 2013; Ciampalini et al. 2014; Yhokha et al. 2015; Razi et al. 2018; Grebby et al. 2019; Figueroa-Miranda et al. 2020) as well as landslide studies from detection to deformation monitoring (Strozzi et al. 2005; Bulmer et al. 2006; Cascini et al. 2010; Calabro et al. 2010; Zhao et al. 2012; Del Ventisette et al. 2013; Wasowski and Bovenga 2014; Zhang et al. 2015; Calò et al. 2015; Casagli et al. 2016; Confuorto et al. 2017; Kyriou and Nikolakopoulos 2018; Zhang et al. 2018; Huang Lin et al. 2019; Aslan et al. 2020; Eker and Aydin 2021).

Remote sensing represents a valuable tool for detecting, mapping, monitoring, and hazard/risk assessment of landslides because field measurements provide only point-based

measurements, even if they are very precise (Hervas et al. 2003). Remote-sensing techniques are used as alternative or complementary methods in landslide studies to compensate for the limitations of field measurements. One of the most common remote-sensing techniques used to investigate landslides is aerial photography (Dewitte et al. 2008; Strozzi et al. 2013). Aerial photographs are used to extract landslide reliefs via digital photogrammetry (Kaab 2002; Baldi et al. 2005; Casson et al. 2005; Hapke 2005; Eker and Aydin 2021). Moreover, the use of the unmanned aerial vehicle (UAV)-based remote sensing for landslide monitoring has increased (Niethammer et al. 2009; Carvajal et al. 2011; Lucieer et al. 2014; Peterman 2015; Turner et al. 2015; Vrublová et al. 2015; Lindner et al. 2016; Tanteri et al. 2017; Mateos et al. 2017; Peternal et al. 2017; Eker et al. 2018; Eker and Aydin 2021). Thus, UAV remote sensing has gained popularity because it provides the advantages of flexibility, low cost, reliability, and autonomy, and the timely delivery of high-resolution data in medium- and small-scale areas (Eker et al. 2018; Matese 2020).

The literature has found studies that have successfully examined ground deformations caused by open-pit mining activities using InSAR time series. Hartwig et al. (2013) evaluated the use of the PSI technique to detect and monitor mine slope deformations in the N4W iron mine and its surroundings in Pará State, northern Brazil. They performed the PSI processing using 18 ascending SAR scenes acquired in the dry season of 2012 from the TerraSAR-X satellite. Mura et al. (2016) aimed to monitor ground deformations based on integrating DInSAR Time-Series (DTS) and PSI techniques in Carajás Mineral Province in the Brazilian Amazon region using a set of 33 TerraSAR-X-1 images acquired from March 2012 to April 2013. Carlà et al. (2018) integrated ground-based radar and satellite InSAR data (Sentinel-1 mission) to analyze an unexpected slope failure in an open-pit mine. Tang et al. (2020) mapped ground displacement and slope instability over three open-pit mines (Hambach, Garzweiler, and Inden) in the Rhenish coalfields of Germany. They applied the SBAS method using Sentinel-1A and TerraSAR-X data, thus providing long-term monitoring solutions for open-pit mining operations and their surroundings. Poyraz et al. (2020) applied the PSI technique using Sentinel-1A data to determine deformations at the common dumpsite of three different open-pit marble mines located in the Eliktekte region of Amasya Province (Turkey).

Due to open-pit coal mining activities, a destructive landslide event occurred at 10:00 pm on 12 Dec 2017 in Himmetoğlu village in Göynük District (Bolu, NW Turkey). Field observations after the landslide failure and interviews with villagers motivated us to question the possibility of using satellite SAR data to detect any signs of failure with regard to deformation velocity. According to the villagers' explanations, the mining activities and subsequent ground deformations had caused increasing cracks in their buildings near the landslide, especially during the three months prior to the failure. Moreover, no earthquake was recorded for the same period within the area with a radius of 150 km. For this reason, the study aimed, first, to map the ground deformations of the recent destructive landslide by applying the DEM of Difference (DoD) method using DEMs obtained from aerial photography and UAV data. However, the primary aim was to track deformation velocity as a sign of landslide failure by mapping ground deformations with PSI and SBAS techniques using Sentinel-1A data from ascending and descending orbits.

2 Material and methods

2.1 Description of the landslide and open-pit mining activities in Himmetoğlu Village

Himmetoğlu, a village in Göynük District (Bolu, NW Turkey), is surrounded by an open-pit coal mining area (Fig. 1). A recent landslide (hereafter referred to as the Himmetoğlu landslide) was triggered by open-pit mining activities at 10:00 pm on 12 Dec 2017. It was a sudden mass collapse stopping its move after failure. Seven houses were damaged due to landslides. One of the houses was completely destroyed, whereas others had slight damage. In addition, large landslide cracks of varying extents had appeared (Fig. 2). The landslide area is located where open-pit mining activities began after the 2014 government expropriation decision (Fig. 3). Following the landslide event, local authorities decided to evacuate these houses immediately. However, instability problems in the region are not new. Since the commencement of mining in the area, serious stability problems have led to interruptions in mining and environmental effects.

The causes, mechanisms, and environmental impact of these instabilities at Himmetoğlu coal mine were investigated over a one-year period in 1997 (Ulusay et al. 2001). According to Ulusay et al. (2001), mining activities in Himmetoğlu began in 1980 at the western end of the coalfield. The Himmetoğlu coal mine, with a reserve of 43 million metric tons of lower-calorific-value lignite, was operated by Turkish Coal Enterprises (TKI) to produce coal for domestic use and for a thermal power plant located 75 km from the pit. The first large slope failure resulting in the interruption of coal production occurred in 1995. Extensive movements were also reported in September 1996 along the south-side wall of the former mining area. In addition, in 1998, new tension cracks extending into agricultural fields as well as many low-seated failures of a few meters in height were reported. These instabilities have influenced the environment surrounding the pit and put agricultural areas under threat. Open-pit mining activities have caused changes in the land cover and land use in the region. In addition to the negative environmental effects, according to the interviews conducted with villagers following the landslide, ground deformations caused by open-pit mining activities had been observed, especially in areas close to the mine. According to the villagers, the mining activities caused damage to their buildings because of these ground deformations. Cracks were observed on both inner and outer walls of the buildings, especially on those located nearby the mining area.

3 Data acquisition

This study aimed to map the landslide deformations of the recent destructive landslide induced by open pit mining activities. However, by mapping the ground deformations in the region, the study was primarily directed at tracking deformation velocity as a sign of landslide failure. Thus, the study included two phases. In Phase 1, the Himmetoğlu landslide was investigated by applying a DEM of Difference (DoD). In Phase 2, the ground deformations in the village were mapped by applying an InSAR time-series analysis using both PSI and SBAS methods.

In the present study, different remote sensing data were used for each phase of the study. For the DoD analysis, the digital elevation model (DEM), including all surface objects

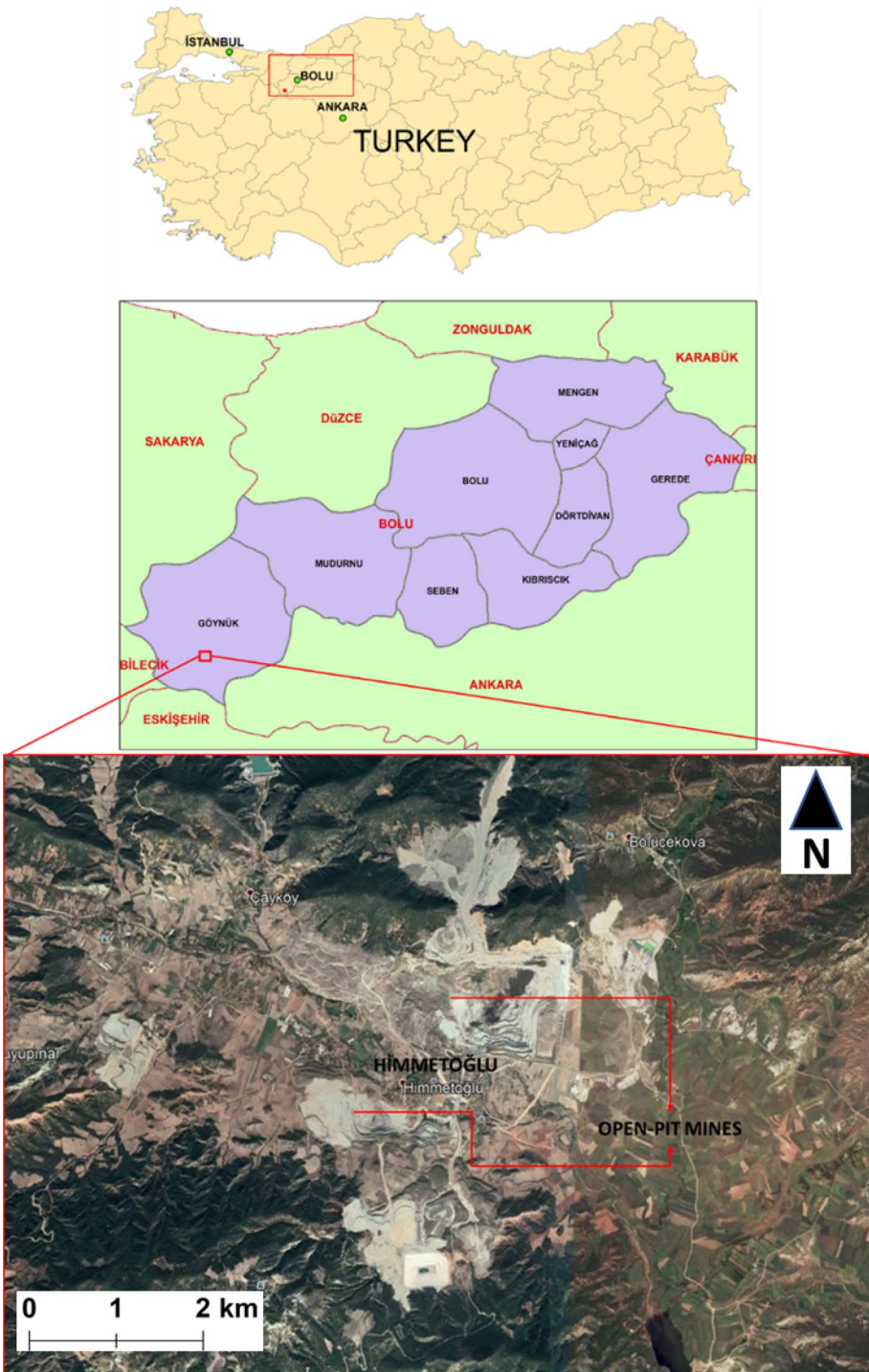


Fig. 1 Location of the study area (corresponds area of interest for InSAR time-series analysis)



Fig. 2 UAV images and photos: (left) landslide cracks and destroyed building, (right) damaged poultry house

(such as buildings and trees, etc.) of the pre-landslide topographical status of the region in 2015 was obtained from the archives of the Turkish General Directorate of Mapping (HGM). The DEM was acquired in GeoTIFF (32 Bit Floating) with 5-m spatial resolution in the UTM-WGS84 spatial reference system. The DEM obtained from HGM was generated with photogrammetric methods using multi-band stereo imageries with 30 cm resolution. There was no information provided by HGM about the precision of DEM data, except the thresholds in spatial accuracies of data as 0.5 m horizontally and 2 m vertically. In addition, a UAV flight was conducted over the landslide area on 17 Dec 2017 in order to generate a high-resolution orthomosaic and DEM of the post-landslide topographical situation. Before applying the DoD, UAV-based DEM was resampled to 5 m resolution, and the root mean square error (RMSE) of the pre- and post-landslide DEMs was calculated using 100 points located over the roofs of buildings, and over ground not covered by vegetation outside the mining and landslide area. A lower value indicated good agreement between the two DEMs. Even though we could not have any field survey to validate 2015 DEM data, we could use UAV data in comparison because we could survey ground control points (GCPs) in the field for its validation.

For the InSAR time-series analysis, a total of 44 C-band (5–6 GHz, ~5.6-cm wavelength) SAR images from the Sentinel-1A satellite (in both ascending and descending orbits: path 160, frame 128 for ascending, and path 65, frame 454 for descending, respectively) were obtained in Level-1 format, i.e., as single-look complex (SLC) data from the archives of the European Space Agency (ESA). While descending orbit data covered the 9-month period before the landslide event, ascending orbit data covered 6-month period (Table 1).

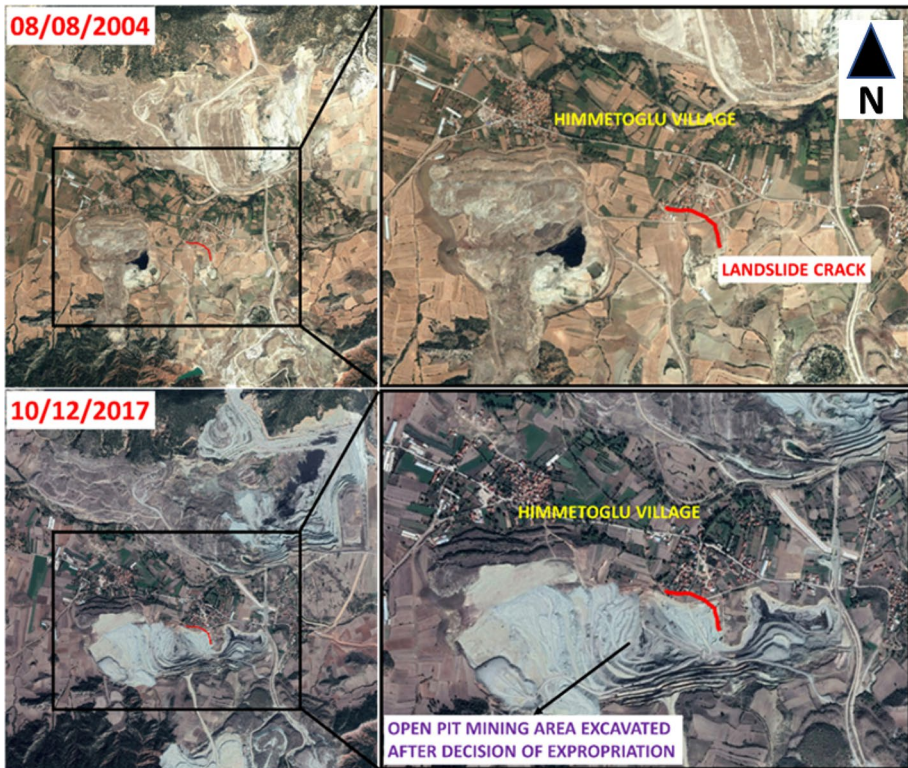


Fig. 3 Google Earth images of before (2004) and after (2017) the commencement of mining activities following the government expropriation decision in 2014

Additionally, daily total precipitation data covering the same period with SAR data acquisition from Göynük Automatic Weather Station (AWS), the closest station to Himmetoğlu village, was obtained. Also, earthquake records from online archives of AFAD (Ministry of Interior Disaster and Emergency Management Presidency) (<https://deprem.afad.gov.tr/>) were investigated for same period. The earthquake records were examined for a region surrounding the Himmetoğlu village as a circle with radius of 150 km.

4 UAV-based image acquisition and data processing

The UAV-based image acquisition was made by following main steps: (1) off-site preparation, (2) on-site preparation and image acquisition, and (3) post-processing (Eker et al. 2018). For the off-site preparation, data collecting about the area, and planning the UAV flight mission were conducted. The Universal Ground Control Software (UgCS) version 2.13.519 was used for flight planning (Fig. 4). For the area of interest, planned UAV mission consist of three flights depending on the spatial resolution and battery limits. All flights were planned with 70% of both front and side overlapping, and at flight altitudes of 100 m a.g.l. (above ground level) for acquiring images with a 3-cm ground sampling distance (GSD). For the on-site preparation and image acquisition stage, in total, the 10

Table 1 Sentinel-1A SAR SLC data obtained from ESA archive

No	Date (descending)	Date (ascending)
1	04-03-2017	02-06-2017
2	16-03-2017	14-06-2017
3	28-03-2017	26-06-2017
4	09-04-2017	08-07-2017
5	21-04-2017	20-07-2017
6	03-05-2017	01-08-2017
7	15-05-2017	13-08-2017
8	27-05-2017	25-08-2017
9	08-06-2017	06-09-2017
10	20-06-2017	18-09-2017
11	02-07-2017	30-09-2017
12	14-07-2017	12-10-2017
13	26-07-2017	24-10-2017
14	07-08-2017	05-11-2017
15	19-08-2017	17-11-2017
16	31-08-2017	29-11-2017
17	12-09-2017	11-12-2017
18	24-09-2017	23-12-2017
19	06-10-2017	
20	18-10-2017	
21	30-10-2017	
22	11-11-2017	
23	23-11-2017	
24	05-12-2017	
25	17-12-2017	
26	29-12-2017	

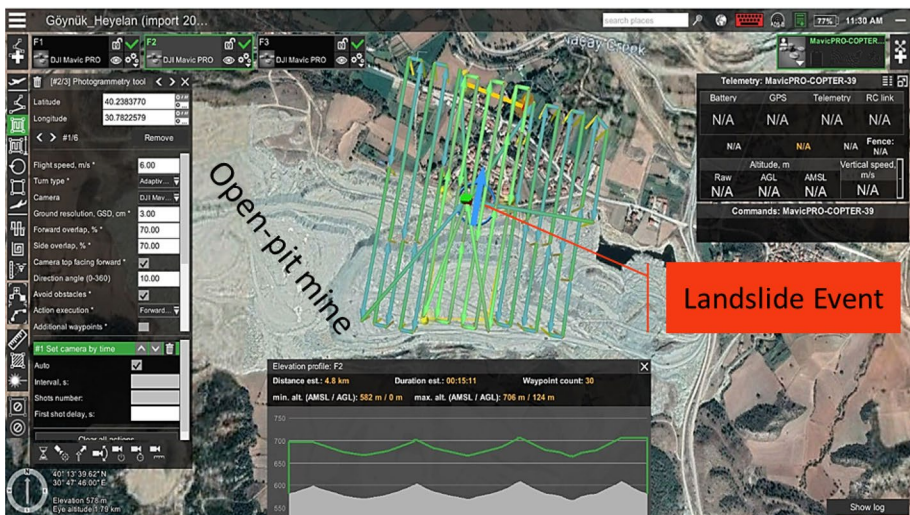


Fig. 4 UAV flight plan prepared using Universal Ground Control Software (UgCS)

GCPs were surveyed with sub-centimeter accuracy with the Satlab SL600 6G GNSS receiver. The rover GNSS receiver was connected to the Turkish RTK CORS Network "TUSAGA-Aktif" to acquire RTK corrections. The UAV platform used for the flights is DJI Mavic Pro platform. This UAV has an integrated CMOS sensor having a resolution of 12 MP. In total, 86 images were taken for the area of interest. For the post-processing, in order to create the high-resolution DEMs (10 cm for this study) and orthomosaics (3 cm for this study) from the UAV images, the structure from motion (SfM) algorithm was applied to generate the DEM and orthomosaic using Agisoft Photoscan Professional version 1.3.2. The generated DEM and orthomosaic are given in Fig. 5.

5 InSAR time-series analysis (PSI and SBAS methods)

In the present study, InSAR time-series analysis were made to determine the ground deformations caused by the open mining activities in Himmetoğlu Village. All SAR data were processed using the SBAS-InSAR algorithm (Berardino et al. 2002) and PSI algorithm (Ferretti et al. 2001), using ENVI 5.3 software (HARRIS Geospatial Solutions) and the SARscape 5.2 module. Only Sentinel-1A data, which is already available in SLC format, was used together with ancillary data obtained from the ESA archives. All data included in the processing (both SLC data and the DEM) need to be imported and transformed into the SARscape format. Due to magnitude of data, it was necessary to clip all SLC data for speeding up the processing chain (Fig. 1). For this aim, a vector file (shapefile) was used in this step. In interferometric analysis, a DEM is needed to simulate and remove the topographic phase contribution to the interferometric process and geocode the resultant InSAR

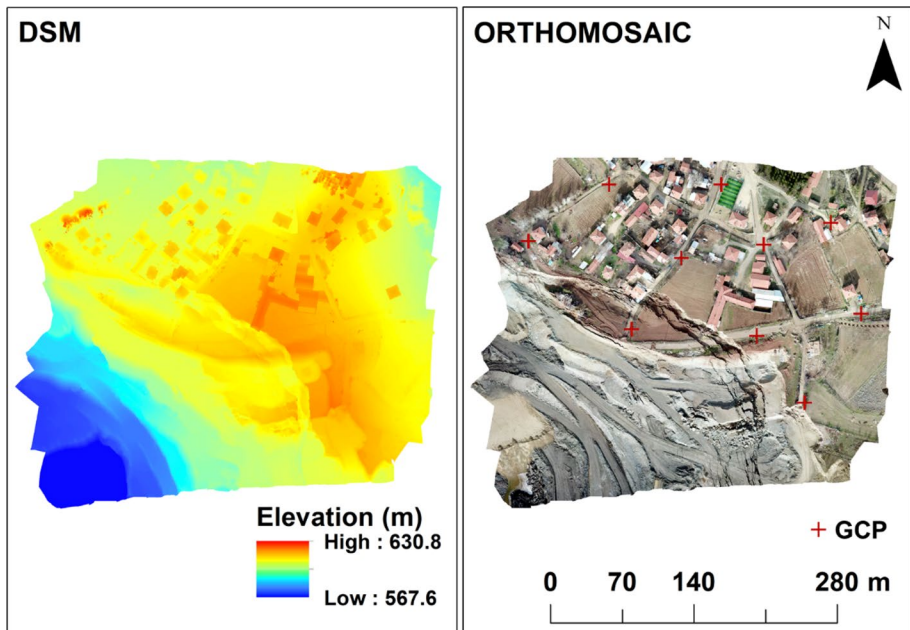


Fig. 5 Generated DEM and Orthomosaic

products from range-Doppler coordinates into map geometry (Hu et al. 2014). The ENVI SARscape module allows downloading a DEM (such as SRTM) of the study area when an Internet connection is available. In the present study, SRTM-3 V2 DEM data with the 30-m terrestrial resolution was downloaded. This was because high resolution DEM used in DoD analysis was available for small area. InSAR time series analysis was applied for a rectangular area given in Fig. 1. All datasets were processed in separate stacks using the interferometric stacking PSI and SBAS workflow. The coherence threshold value (γ) for filtering results was set as $\gamma \geq 0.7$ for PSI and $\gamma \geq 0.2$ for SBAS methods.

6 Results and discussion

6.1 Results of DoD analysis for landslide investigation

A DoD analysis was applied to assess landslide deformations. For this, a 5-m DEM representing the 2015 pre-landslide topographical status was obtained from the HGM, and a UAV-based DEM representing the 2017 post-landslide topographical situation was used. Landslide deformations were mapped, as shown in Fig. 6. The deformation map resulting from the DoD was filtered between 1 m and -20 m because we surely knew that there was no uplifting higher than 1 m in the region. The DoD values higher than 1 m were due to vegetation existence as a group of trees. Figure 7 shows the profile graphs of the road destroyed by the landslide. The landslide occurred as slumping caused by the open-pit mining excavations in the region. The landslide crown cracks reached up to 25 m in width and 10 m in depth. Both the obtained and generated DEMs

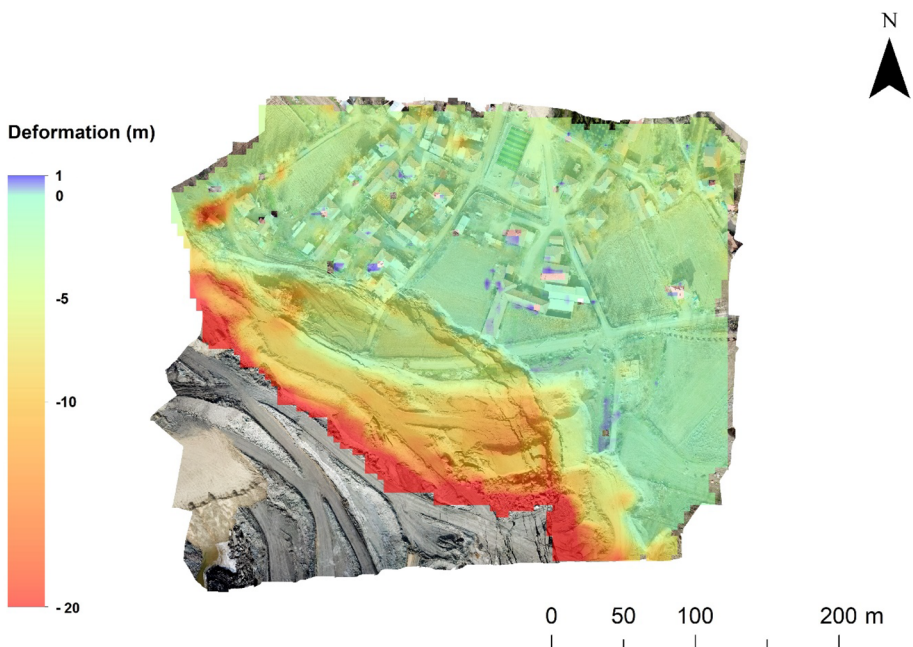


Fig. 6 Results of DoD methods showing landslide deformations in the Z direction

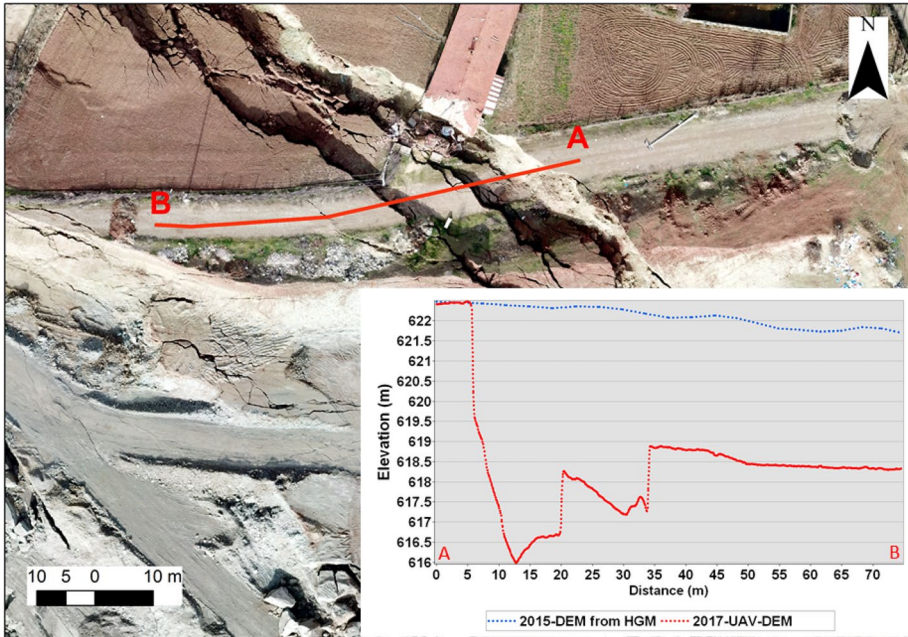


Fig. 7 Profile graph (from point A to point B) of road destroyed by the landslide

of the landslide enabled the mapping of the landslide deformations. The DoD results enabled the estimation of the volume of the moving landslide mass covering a 3D surface area of $25,251.95 \text{ m}^2$ as $106,160.34 \text{ m}^3$. Thus, the study achieved a successful application of the DoD analysis. The DoD analysis is a straightforward method used by many researchers in the literature (e.g., Lucieer et al. 2014; Turner et al. 2015; Eker et al. 2018; Kim et al. 2020) to provide measured values of vertical distance on a pixel-by-pixel basis. The current study represents an impressive case study demonstrating the use of remote sensing to investigate a landslide triggered by open-pit mining activities when terrestrial topographical surveys were lacking. Therefore, the deficiencies of survey data were remedied by the combined use of DEMs generated from digital aerial images taken by manned aircraft and images taken via UAVs. However, it should be noted that when using photogrammetric methods, some errors will be present in the generated DEMs. As Prokešová et al. (2010) stated, errors and resulting uncertainty can never be fully eliminated in spatial data. For this reason, before the DoD analysis, a comparison of DEMs should be made from points where Z values remain unchanged despite landslides or excavations (Eker et al. 2018). In this study, the RMSE (i.e., the difference in Z values between DEM points) was 35 cm. This means that the DoD RMSE value of $\pm 35 \text{ cm}$ could have resulted from modeling errors. In literature, the accuracy of DEMs has also been evaluated using checkpoints, which can be installed as stabilized pillars of the geodetic network within the area of interest (Prokešová et al. 2010). However, such checkpoints should be installed and surveyed on the same date as the acquisition date of remote sensing data. In the present study, only GCPs were surveyed for UAV-based image acquisition and data processing. The DEM representing

the 2015 pre-landslide topographical status was obtained from the HGM in 2018. That's why, there was no way to survey checkpoints for a retrospective period.

7 Results of InSAR time-series analysis for ground deformation investigation

In this study, both PSI and SBAS methods (Sentinel-1A satellite C-band SAR data in ascending and descending orbits) were applied to determine the ground deformations. While SAR data in descending orbit covered 9 months (from 01.03.2017 to 31.12.2017), SAR data in ascending orbit covered a 6-month period (from 01.06.2017 to 31.12.2017). In total, 26 SAR data in descending orbit was able to be used, whereas 18 SAR data in ascending orbit was able to be used. This was due to the existence of two different frames (128 and 132) in the same path involving the study area. In ascending orbit, Sentinel-1A data prior to the sixth month (June) was available in the "frame 132" having a significant positional difference in the azimuth direction, so that caused errors in processing with "Interferometric Stacking" tool of SARscape module. That's why we had to exclude them from the analysis. In the PSI method with SARscape module, the identification of PS points is generally considered reliable when 20 or more acquisitions are used (Sarmap 2014). But, in the SBAS method with the SARscape module, the minimum number of acquisitions should be 12–15 (Sarmap 2013). However, when the displacement rates were investigated in Fig. 13, a similar displacement trend was observed for both PSI and SBAS methods. This study used only Sentinel-1A SAR data obtained from ESA archives. In recent studies in the literature, Sentinel-1 satellite C-band SAR data has been the most commonly selected SAR data (Carlà et al. 2018; Poyraz et al. 2020), although TerraSAR-X data has also been used (Hartwig et al. 2013; Tang et al. 2020). Sentinel-1 data couple favorable characteristics such as short visiting time, regional-scale mapping capability (due to the large swath, 250 km), systematic and regular SAR acquisitions, rapid product delivery, and free of charge (Intrieri et al. 2018).

According to the results obtained via SBAS analysis, the deformation velocity for ascending and descending orbits varied between -12 and 39 mm year⁻¹ and between -24 and 6 mm year⁻¹, respectively. The "Vprecision" values of PS points were obtained as 3.32 mm/year. "Vprecision" values correspond to the estimate of the velocity measurement average precision in millimeter/year (Sarmap 2014). The number of PS points detected directly within the settlement area close to the landslide was more for ascending orbit data than for descending orbit (Fig. 8). In addition, a gradual increase in deformation velocity was more clearly observed from far towards closer points to landslide crack with SAR data in ascending orbit (Fig. 8). According to results obtained via the PSI method, the deformation velocity for ascending and descending orbits varied between -16 and 31 mm year⁻¹ and between -18 and 20 mm year⁻¹, respectively. The "Vprecision" values of PS points were obtained as 2.92 mm/year. In contrast to SBAS analysis, the number of PS points detected directly within the settlement area was more for descending than ascending orbit (Fig. 9). In the study, InSAR time-series analysis results indicated that ground deformations at all detected PS points showed a higher velocity in the locations near the landslide crack (Figs. 8 and 9). Here, a positive sign means a decrease of the sensor-to-target slant range distance, whereas a negative sign means an increase of the sensor-to-target slant range distance. When the displacements from both orbits are compared, the opposite directions are detected (Figs. 12 and 13). This can be explained as that in the

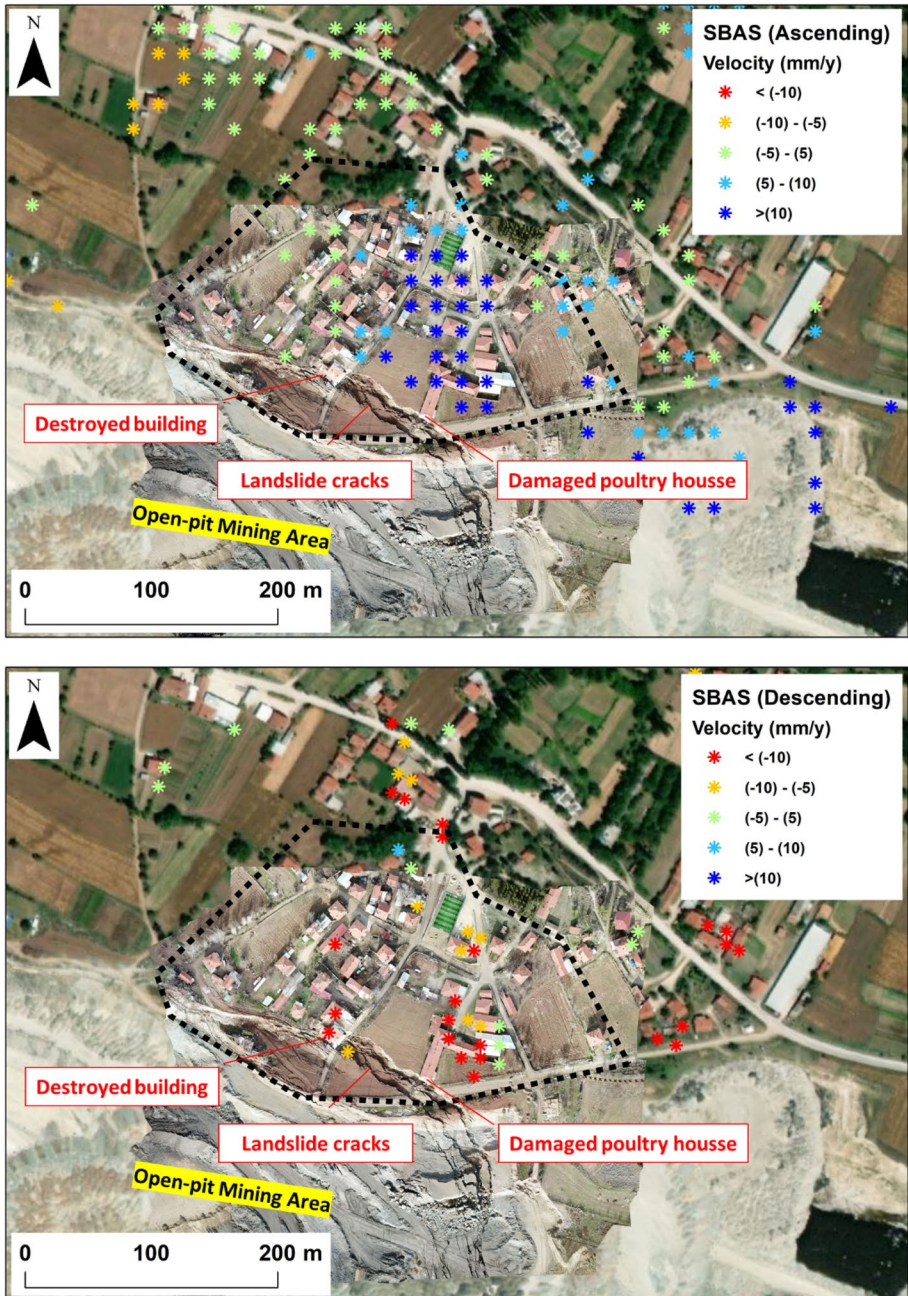


Fig. 8 Results of SBAS analysis performed for the region

region the displacements are dominantly in horizontal direction than vertical direction. Because, if the displacements had been as subsidence or uplifting only in Z direction,

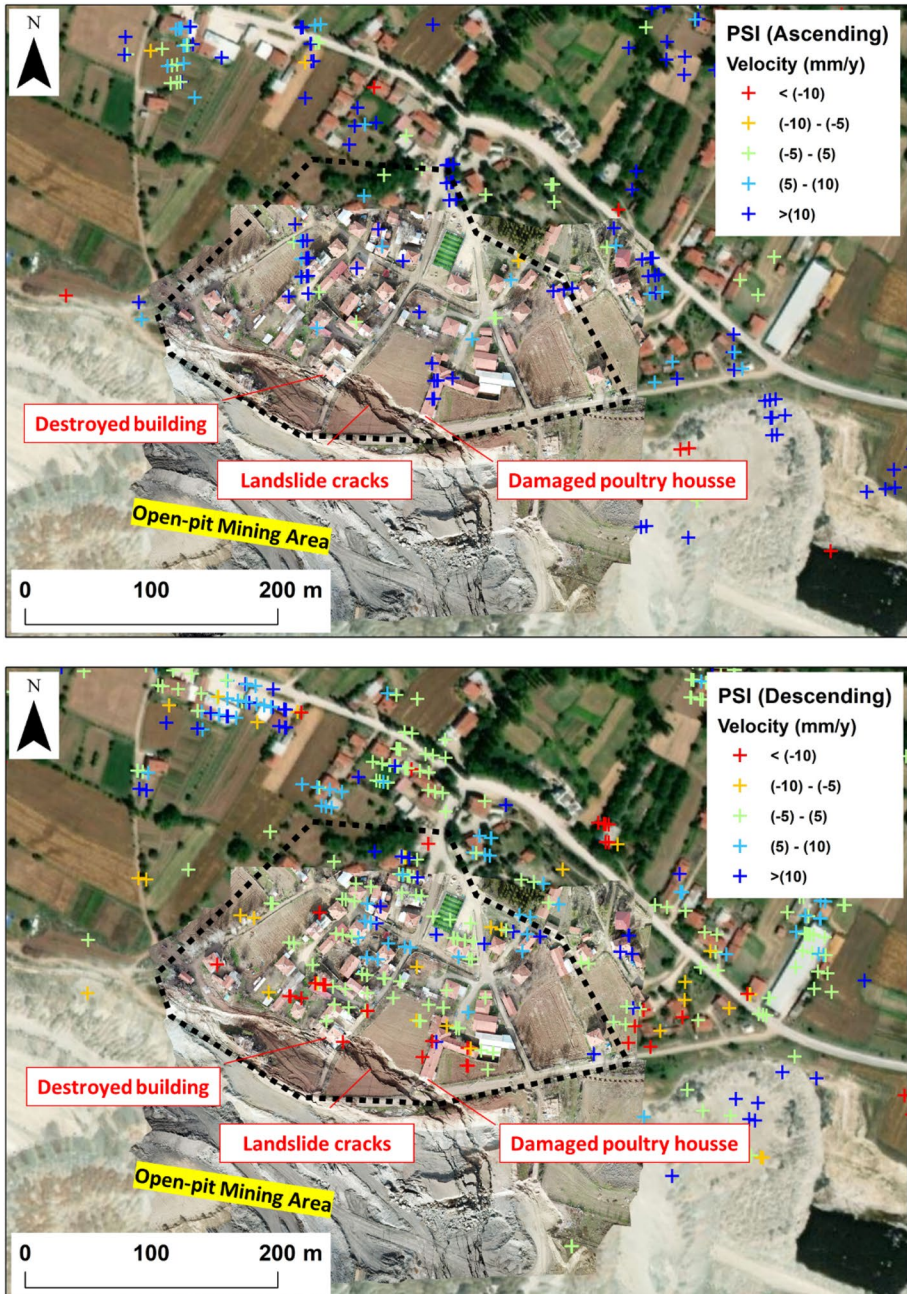


Fig. 9 PSI results for the region

the interferometric analysis from both orbits had should be resulted in same directional deformations.

In descending orbit, the PS number and spatial density obtained by PSI in the settlement area were significantly higher than SBAS method when the coherence threshold value (γ) was set as $\gamma \geq 0.7$ for PSI and set as $\gamma \geq 0.2$ for SBAS method. But on the other hand, in ascending orbit, fewer PS numbers were detected by PSI method than SBAS method. This can be due to PSI focuses on so-called Point Targets, which are objects possibly of small size and with a very well characterized geometry like corner reflectors (e.g., buildings, rocks) and with a high temporal stability of the backscattered signal; the SBAS vice-versa concentrates the analysis on so-called distributed targets, like open fields and not very geometrically characterized objects (Pasquali et al. 2014). Temporal decorrelation is considered an important factor affecting the accuracy of the measured displacements on PS points. The number of PS points depends on the characteristics of the observed areas in relationship with the system wavelength. It is well known that repeat pass SAR acquisitions show a very high correlation over point targets and man-made features, independently from system wavelength (Crosetto et al. 2010, 2016). The availability of buildings in the area enables us to make an InSAR analysis with a high interferometric correlation.

It was observed that the results of both the PSI and SBAS methods obtained from Sentinel-1 data were compatible with the field observations and the interviews with the villagers whose buildings had been damaged. According to the villagers, the mining activities caused damage to their buildings via ground deformations, especially over the three months prior to the failure. Cracks were observed on both inner and outer walls of the buildings, especially for those located near the mining area. Two explicit samples of cracks in buildings observed in the village are given in Figs. 10, 11. According to the owner of the building shown in Fig. 11, the cracks were formed after the mining activities triggered the landslide. The PS point detected over the building showed deformation velocity values ranging between 10 and 15 mm year⁻¹, which corresponded to the higher deformation velocities in ascending orbit. Similarly, the PS point detected over the building given in Fig. 10 exhibited deformation velocity values ranging between -24 and -15 mm year⁻¹, which corresponded to the highest deformation velocities in descending orbit. These results demonstrated that the damage to buildings showed a good correlation with the deformation velocity detected from Sentinel-1 SAR data. However, in this study, no observation provides an answer to which InSAR method results in deformations more correctly. According to Pasquali et al. (2014), the PSI method is very accurate on PS, whereas SBAS is slightly less accurate. In addition, the InSAR techniques can measure only the LOS (line of sight) direction component of the actual movement (Silvia et al. 2013; Barra et al. 2017). It means that slope orientation and inclination with respect to the LOS direction mainly control the performance of PSI analysis. It is not sensible to N-S displacement. In case of the deformation, direction is perpendicular to the satellite LOS, the real movement will be measured as zero. That's why, it is necessary to combine SAR scenes acquired from both ascending and descending orbits. In this study, both ascending and descending orbit SAR data was used, and the results were obtained as compatible with observations. Therefore, the flat topography of the study area can be considered a property that minimizes biases in detecting movement by applying InSAR methods. There is no geometrical limitation for the study area in relation to the SAR data acquisition geometry in topography. These limitations are shadow zones, where the slope is not seen by the radar beam (no radar visibility), and foreshortening zones, where the hillslope is almost parallel to the wave-front. Another limitation of the PSI and SBAS techniques is maximum detectable displacement, which depends on the electromagnetic wavelength, the temporal resolution, and the spatial density of the scatterers (Hartwig et al. 2013). The temporal decorrelation of the SAR scenes, phase unwrapping problems, and spatial gaps among

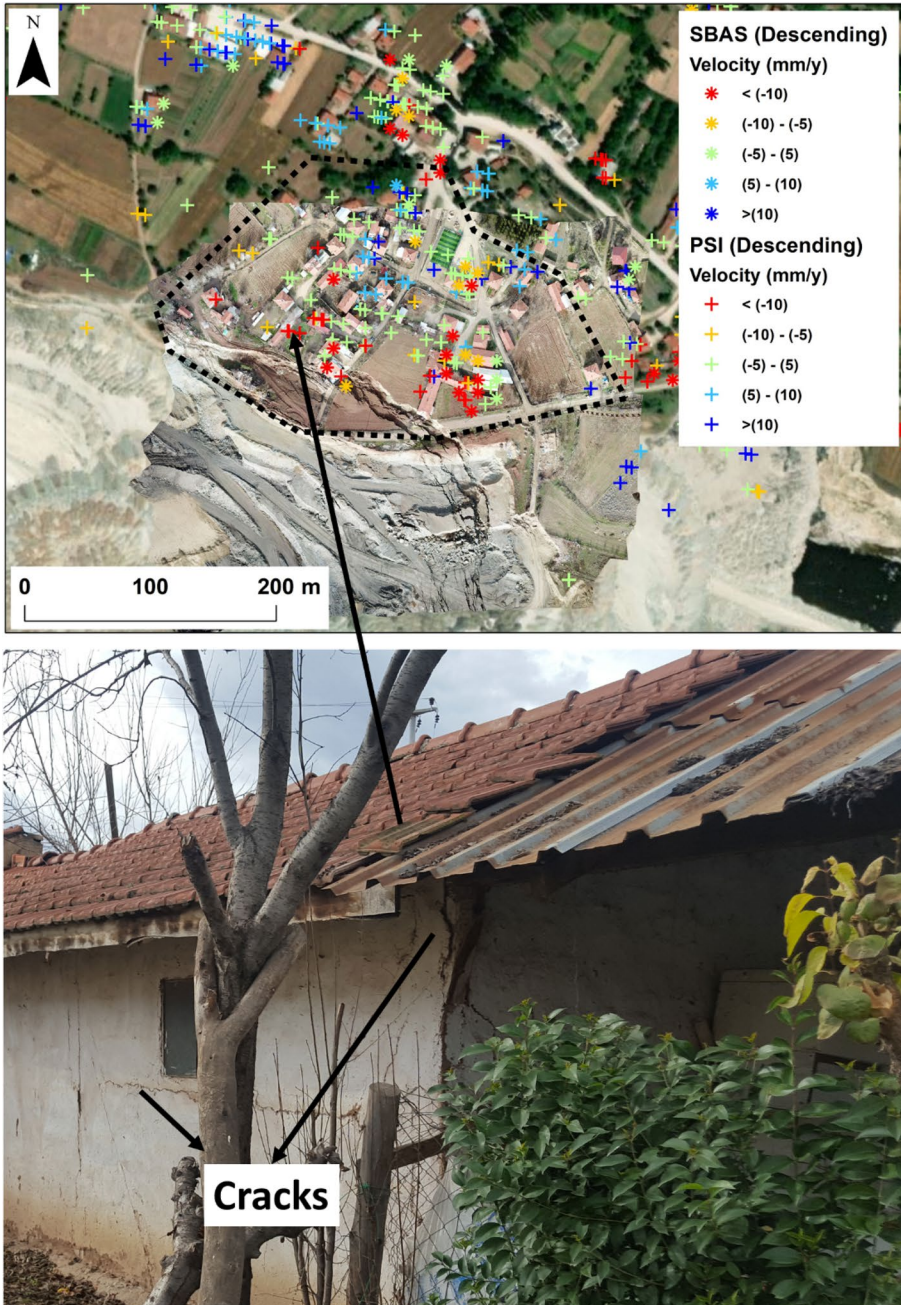


Fig. 10 Cracks observed on the outer wall of a cowshed located close to the landslide crown

scatterers are other factors posing substantial restrictions to the use of the PSI and SBAS techniques (Colesanti and Wasowski 2006).

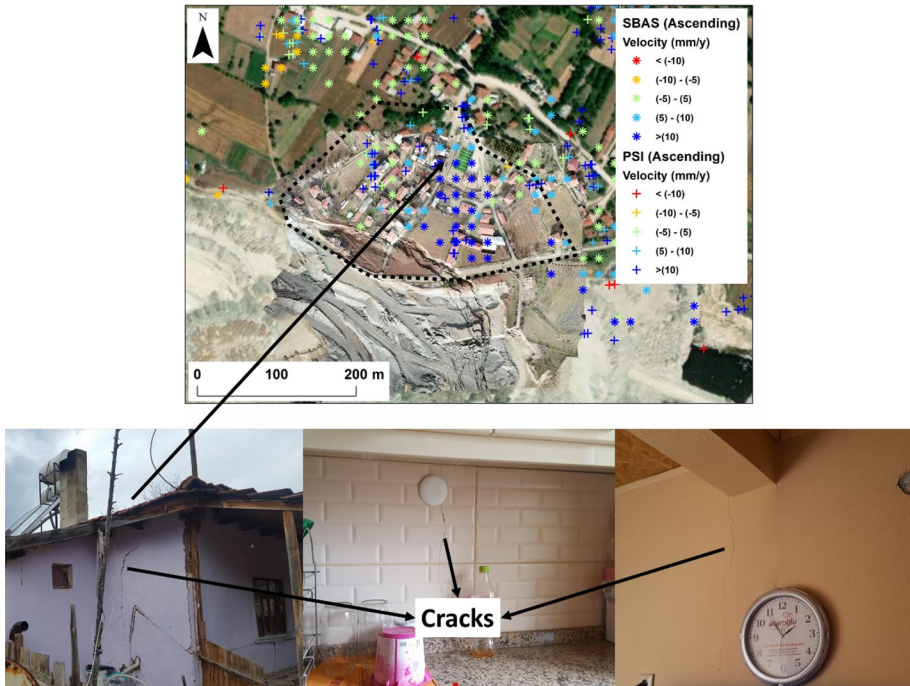


Fig. 11 Cracks observed in a building located 132 m from the landslide crown where deformation velocities are high: (left) on outer wall, (middle and right) on inner walls

The InSAR time-series analysis allowed the creation of displacement graphs of the PS points for the data acquisition period. The daily total precipitation was also integrated into graphs. Thus, any evidence of a landslide before its occurrence could be examined regarding the ground displacement estimated by the InSAR analysis. Time-series displacements of four selected PS points in descending orbit, two of them located near the area where the building was destroyed by the landslide and the remaining two near the poultry house that was damaged, are given in Fig. 12. The graphs in Fig. 12 show that the displacement rates at the points detected by PSI and SBAS changed sharply especially after 12.09.2017, which corresponds a period of three months prior to the landslide. Also, in here, a significant increase in precipitation after same date was observed, but there was no any earthquake recorded. It can be resulted that gradually increasing mining activities together with contribution of precipitation playing a significant role in such sharp change in displacement rate. Figure 14 shows how the border of the mining area expanded towards the village due to mining activities. A similar situation in Fig. 12 was also observed at the PS points in Fig. 13. These graphs show the time series of displacement rates at selected four points in ascending orbit. When two points located over the poultry house are investigated, near the points selected in descending orbit, a very similar trend in time series of displacement but in the opposite direction could be seen. The observed acceleration of ground deformation at selected PS points subscribes to the idea of the use of InSAR time-series analysis for detecting precursors of a landslide failure. For instance, Intrieri et al. (2018) already used Sentinel-1 data for detecting precursors of Maoxian landslide, occurred in the

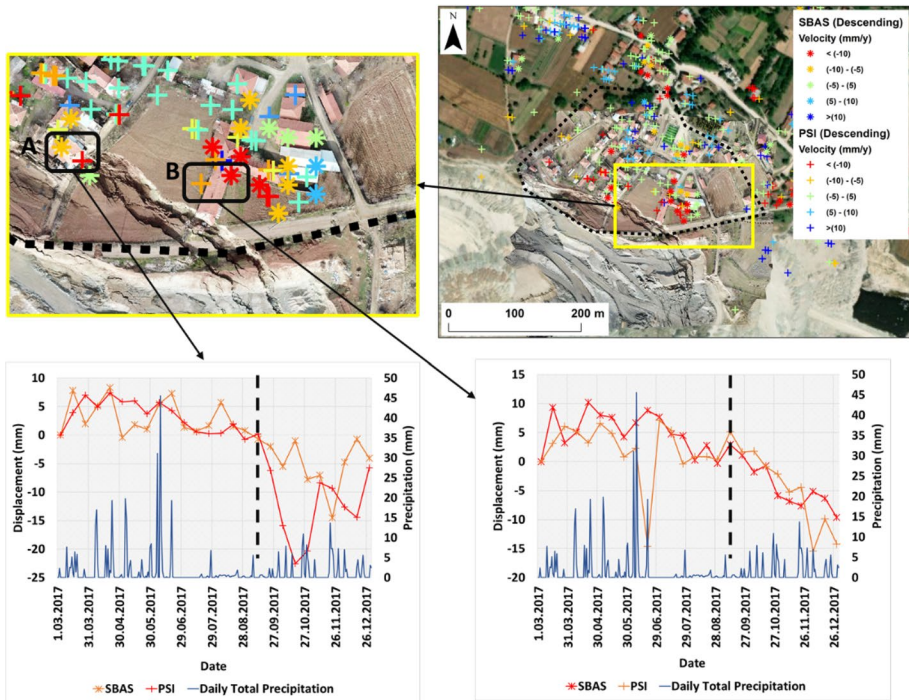


Fig. 12 Time-series vertical displacement (descending orbit) at two PS points over destroyed building (A) and two PS points over damaged poultry house (B) together with daily total precipitation (mm). Vertical dashed line corresponds to the date of SAR acquisition on 12.09.2017

Sichuan province (China) on 24 June 2017, for early warning purposes. They stated that displacement time series in the area of the main scarp of the landslide revealed pre-failure signs with an apparent acceleration from late April 2017, corresponding to the last 180 days of the time series. In this study, the acceleration was observed in previous three months. They resulted that satellite radar data is possible for the early identification of any anomalous trend and/or acceleration of ground deformation even without any in situ survey. Even though a comprehensive method, such as trend variation analysis, was not used to analyze the anomalous trend and/or acceleration of ground deformation in the present study, visual inspection revealed a clear sign of failure with respect to deformation velocities. However, it should be paid sufficient attention that such ground deformations cannot always be evaluated as signs of potential slope failures that can be occurred. So that, monitoring such ground deformations should be made carefully by observing the progress in mining activities and other factors such as rainfall and earthquakes. This study resulted that SAR interferometric time series analysis has the makings of being used as suitable approach in early discerning and avoiding such slope failures in open mining areas (Fig. 14).

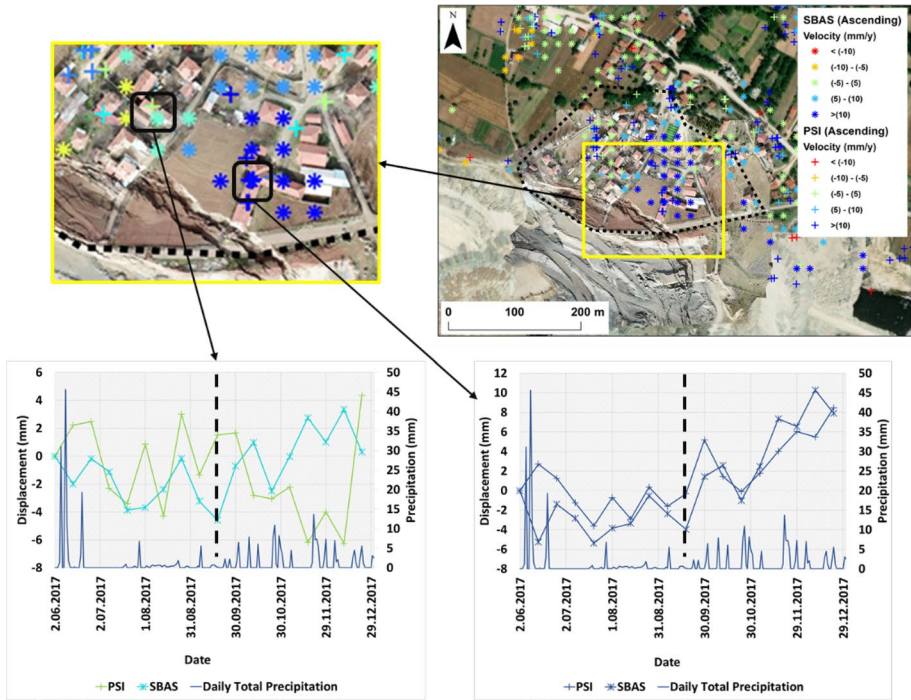


Fig. 13 Time-series vertical displacement (ascending orbit) at two PS points over a building at distance of 45 m to destroyed building and two PS points over damaged poultry house (B) together with daily total precipitation (mm). Vertical dashed line corresponds to the date of SAR acquisition on 18.09.2017

8 Conclusions

Himmetoğlu village is surrounded by open-pit mining areas where coal-mining operations have been carried out since the 1980s. The latest mining activities began at the southern part of the village following the 2014 decision of the government to expropriate the mines. These intensive mining activities around the village have caused several environmental problems, the main one being ground deformation. In addition, the mining activities triggered a destructive landslide event resulting in severe damage to buildings. The present study presented the use of different remote sensing data in the investigation of the recent destructive landslide and ground deformation caused by the open-pit mining activities in Himmetoğlu. The DoD method was selected and applied using DEMs representing the region's pre-and post-landslide topographic status. The pre-landslide topographic situation was obtained from the HGM as DEM data generated from digital aerial images via photogrammetric methods. The post-landslide topographical situation was created as a DEM via a UAV-based photogrammetric method. The availability of both data enabled the investigation of the landslide deformation. The deformation was successfully mapped using remote sensing techniques even though field surveys were lacking.

In addition, both PSI and SBAS methods were applied using Sentinel-1A SAR data to map ground deformation in the village. The SAR data acquisition covered the 9 months before the landslide. Ground deformations at higher velocities were found at locations near

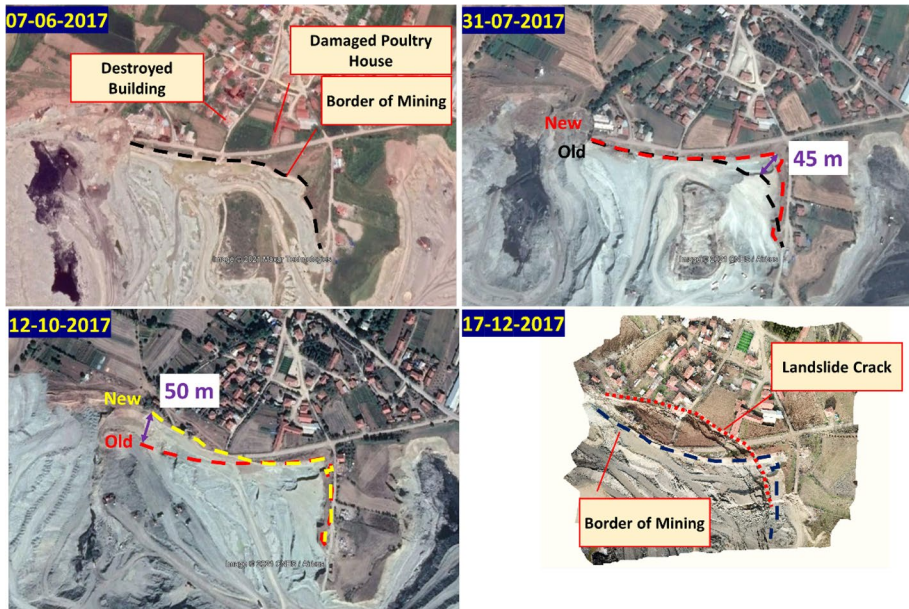


Fig. 14 Temporal change in border of mining area from 07.06.2017 to 12.10.2017 and its last situation in landslide occurrence. While "Old" shows the border of mining in acquisition time of previous image, "New" shows the border of mining in acquisition time of current image. So that, it can be clearly observed how mining area expanded towards to village due to mining activities

the landslide crown. Moreover, most cracks on inner and outer walls were observed in buildings located where deformation velocities were higher. The results of the InSAR time-series analysis were compatible with the field observations and interviews with villagers whose buildings had been damaged. The study concluded that InSAR time-series analysis also enables evidence of landsliding in terms of ground displacement to be investigated before ultimate failure occurs. Higher displacements were observed over three months before the landslide. These higher displacements were assumed to be signs of landslide failure, since the small errors in velocity map, which our study has lower than 4 mm precision of velocity. Consequently, it was concluded that interferometric SAR methods could be used to evaluate the risk of slope failures at the perimeters of open-pit mining areas. It is recommended that directors/technicians of open-pit mining corporations use these methods for regular monitoring of ground deformations around the mining area to minimize the risk of such a slope failure.

Authors' Contributions RE: Conceptualization, Methodology, Software, Data curation, Writing- Original draft preparation. AA: Conceptualization, Supervision, Writing—Review & Editing. TG: Supervision, Review & Editing.

Funding Open access funding provided by the Scientific and Technological Research Council of Türkiye (TÜBİTAK).

Declarations

Conflicts of interest The authors declare that they have no known competing financial interests or personal relationships that could have appeared to influence the work reported in this paper.

Open Access This article is licensed under a Creative Commons Attribution 4.0 International License, which permits use, sharing, adaptation, distribution and reproduction in any medium or format, as long as you give appropriate credit to the original author(s) and the source, provide a link to the Creative Commons licence, and indicate if changes were made. The images or other third party material in this article are included in the article's Creative Commons licence, unless indicated otherwise in a credit line to the material. If material is not included in the article's Creative Commons licence and your intended use is not permitted by statutory regulation or exceeds the permitted use, you will need to obtain permission directly from the copyright holder. To view a copy of this licence, visit <http://creativecommons.org/licenses/by/4.0/>.

References

- Aly MH, Zebker A, Giardino JR, Klein AG (2009) Permanent scatterer investigation of land subsidence in Greater Cairo. *Egypt Geophys J Int* 178:1238–1245
- Aobpaet A, Cuenca MC, Hooper A, Trisirisatayawong I (2013) InSAR time-series analysis of land subsidence in Bangkok. *Thail Int J Remote Sens* 34(8):2969–2982
- Aslan G, Fomelis M, Raucoules D, De Michele M, Bernardie S, Cakir Z (2020) Landslide mapping and monitoring using persistent scatterer interferometry (PSI) technique in the French Alps. *Remote Sens* 12(8):1305
- Baldi P, Fabris M, Marsella M, Monticelli R (2005) Monitoring the morphological evolution of the Sciarà del Fuoco during the 2002–2003 Stromboli eruption using multi-temporal photogrammetry. *ISPRS J Photogramm Remote Sens* 59(4):199–211
- Barra A, Solari L, Béjar-Pizarro M, Monserrat O, Silvia Bianchini S, Herrera G, Crosetto M, Sarro R, González-Alonso E, Mateos RM, Ligüerzana S, López C, Moretti S (2017) A methodology to detect and update active deformation areas based on Sentinel-1 SAR images. *Remote Sens* 9(10):1002
- Berardino P, Fornaro G, Lanari R, Sansosti E (2002) A new algorithm for surface deformation monitoring based on small baseline differential SAR interferograms. *IEEE Trans Geosci Remote Sens* 40:2375–2383
- Bulmer MH, Petley DN, Murphy W, Mantovani F (2006) Detecting slope deformation using two-pass differential interferometry: implications for landslide studies on Earth and other planetary bodies. *J Geophys Res* 111:E06S16
- Calabro MD, Schmidt DA, Roering JJ (2010) An examination of seasonal deformation at the Portuguese Bend landslide, southern California, using radar interferometry. *J Geophys Res* 115:F02020
- Calò F, Abdikan S, Görüm T, Pepe A, Kiliç H, Balik Şanlı F (2015) The space-borne SBAS-DInSAR technique as a supporting tool for sustainable urban policies: the case of Istanbul Megacity. *Turkey Remote Sens* 7(12):16519–16536
- Canova F, Tolomei C, Salvi S, Toscani G, Seno S (2012) Land subsidence along the Ionian coast of SE Sicily (Italy), detection and analysis via Small Baseline Subset (SBAS) multitemporal differential SAR interferometry. *Earth Surf Proc Land* 37:273–286
- Carlà T, Farina P, Intrieri E, Ketizmen H, Casagli N (2018) Integration of ground-based radar and satellite InSAR data for the analysis of an unexpected slope failure in an open-pit mine. *Eng Geol* 235:39–52
- Carvajal F, Agüera F, Pérez M (2011) Surveying a landslide in a road embankment using unmanned aerial vehicle photogrammetry. *Int Arch the Photogramm Remote Sens Spat Inf Sci XXXVIII, Part 1(C22):201–206*
- Casagli N, Cigna F, Bianchini S, Hölbling D, Füreder P, Righini G, Del Conte S, Friedl B, Schneiderbauer S, Iasio C, Vlcko J, Greif V, Prose H, Granica K, Falco S, Lozzi S, Mora O, Arnaud A, Novali F, Bianchi M (2016) Landslide mapping and monitoring by using radar and optical remote sensing: examples from the EC-FP7 project SAFER. *Remote Sens Appl Soc Environ* 4:92–108
- Cascini L, Fornaro G, Peduto D (2010) Advanced low- and full-resolution DInSAR map generation for slow-moving landslide analysis at different scales. *Eng Geol* 112:29–42

- Casson B, Delacourt C, Allemand P (2005) Contribution of multi-temporal remote sensing images to characterize landslide slip surface—application to the La Clapiere landslide, France. *Nat Hazard* 5(3):425–437
- Chen F, Lin H, Zhou W, Hong T, Wang G (2013) Surface deformation detected by ALOS PALSAR small baseline SAR interferometry over permafrost environment of Beiluhe section, Tibet Plateau, China. *Remote Sens Environ* 138:10–18
- Ciampalini A, Bardi F, Bianchini S, Frodella W, Del Ventisette C, Moretti S, Casagli N (2014) Analysis of building deformation in landslide area using multisensory PSInSAR™ technique. *Int J Appl Earth Obs Geoinf* 33:166–180
- Colesanti C, Wasowski J (2006) Investigating landslides with space-borne Synthetic Aperture Radar (SAR) interferometry. *Eng Geol* 88:173–199
- Confuorto P, Di Martire D, Centolanza G, Iglesias R, Mallorqui JJ, Novellino A, Plank S, Ramondini M, Thuro K, Calcaterra D (2017) Post-failure evolution analysis of a rainfall-triggered landslide by multi-temporal interferometry SAR approaches integrated with geotechnical analysis. *Remote Sens Environ* 188:51–72
- Crosetto M, Monserrat O, Iglesias R, Crippa B (2010) Persistent Scatterer Interferometry: Potential, limits and initial C- and X-band comparison. *Photogramm Eng Remote Sens* 76:1061–1069
- Crosetto M, Monserrat O, Cuevas-González M, Devanthery N, Crippa B (2016) Persistent scatterer interferometry: A review. *ISPRS J Photogramm Remote Sens* 115:78–89
- Del Ventisette C, Ciampalini A, Manunta M, Calò F, Paglia L, Ardizzone F, Mondini AC, Reichembach P, Mateos RM, Bianchini S, Garcia I, Füsi B, Deak ZV, Radi K, Graniczny M, Kowalski Z, Piatkowska A, Przylucka M, Retzo H, Strozzi T, Colombo D, Mora O, Sanches F, Herrera G, Moretti S, Casagli S, Guzzetti F (2013) Exploitation of large archives of ERS and ENVISAT C-band SAR data to characterize ground deformations. *Remote Sens* 5(8):3896–3917
- Demirel N, Düzgün S, Emil MK (2011) Landuse change detection in a surface coal mine area using multi-temporal high-resolution satellite images. *Int J Min Reclam Environ* 25(4):342–349
- Dewitte O, Jasselette JC, Cornet Y, Van Den Eeckhaut M, Collignon A, Poesen J, Demoulin A (2008) Tracking landslide displacements in multi-temporal DTMs: A combined aerial stereophotogrammetric and LIDAR approach in western Belgium. *Eng Geol* 99:11–22
- Eker R, Aydın A (2021) Long-term retrospective investigation of a large, deep-seated, and slow-moving landslide using InSAR time series, historical aerial photographs, and UAV data: The case of Devrek landslide (NW Turkey). *CATENA* 196:104895
- Eker R, Aydın A, Hübl J (2018) Unmanned aerial vehicle (UAV)-based monitoring of a landslide: Gallenzerkogel landslide (Ybbs-Lower Austria) case study. *Environ Monit Assess* 190:28
- Ferretti A, Prati C, Rocca F (2001) Permanent scatterers in SAR interferometry. *IEEE Trans Geosci Remote Sens* 39:8–20
- Figueroa-Miranda S, Hernández-Madrigal VM, Tuxpan-Vargas J, Villaseñor-Reyes CI (2020) Evolution assessment of structurally-controlled differential subsidence using SBAS and PS interferometry in an emblematic case in Central Mexico. *Eng Geol* 279:105860
- Friedl B, Hölbling D (2015) Using SAR interferograms and coherence images for object-based delineation of unstable slopes. *FRINGE 2015 workshop: advances in the science and applications of SAR interferometry and Sentinel-1 InSAR Workshop*, 23–27 March. Frascati, Italy, p 6
- Gourmelen N, Amelung F, Casu F, Manzo M, Lanari R (2007) Mining-related ground deformation in Crescent Valley, Nevada: Implications for sparse GPS networks. *Geophys Res Lett* 34:L09309
- Grebby S, Orynbassarova E, Sowter A, Gee D, Athab A (2019) Delineating ground deformation over the Tengiz oil field, Kazakhstan, using the Intermittent SBAS (ISBAS) DInSAR algorithm. *Int J Appl Earth Obs Geoinf* 81:37–46
- Hapke CJ (2005) Estimation of regional material yield from coastal landslides based on historical digital terrain modelling. *Earth Surf Proc Land* 30(6):679–697
- Hartwig ME, Paradella WR, Mura JC (2013) Detection and monitoring of surface motions in active open pit iron mine in the amazon region, using persistent scatterer interferometry with TerraSAR-X satellite data. *Remote Sens* 5(9):4719–4734
- Herrera G, Tomas R, Vicente F, Lopez-Sanchez JM, Mallorqui JJ, Mulas J (2010) Mapping ground movements in open pit mining areas using differential SAR interferometry. *Int J Rock Mech Min Sci* 47(7):1114–1125
- Hervas J, Barredo JJ, Rosin PL, Pasuto A, Mantovani F, Silvano S (2003) Monitoring landslides from optical remotely sensed imagery: the case history of Tessina landslide Italy. *Geomorphology* 54(1–2):63–75
- Hu J, Li ZW, Ding XL, Zhu JJ, Zhang L, Sun Q (2014) Resolving three-dimensional surface displacements from InSAR measurements: a review. *Earth-Sci Rev* 133:1–17

- Huang Lin C, Liu D, Liu G (2019) Landslide detection in La Paz City (Bolivia) based on time series analysis of InSAR data. *Int J Remote Sens* 40(17):6775–6795
- Intrieri E, Raspini F, Fumagalli A, Lu P, Del Conte S, Farina P, Allievi J, Ferretti A, Casagli N (2018) The Maoxian landslide as seen from space: detecting precursors of failure with Sentinel-1 data. *Landslides* 15(1):123–133
- Intrieri E, Carlà T, Farina P, Bardi F, Ketizmen H, Casagli N (2019) Satellite interferometry as a tool for early warning and aiding decision making in an open pit mine. *IEEE J Sel Top Appl Earth Observ Remote Sens* 12(12):5248–5258
- Kaab A (2002) Monitoring high-mountain terrain deformation from repeated air- and space-borne optical data: examples using digital aerial imagery and ASTER data. *ISPRS J Photogramm Remote Sens* 57:39–52
- Kim, MK, Sohn HG, Kim S (2020) Incorporating the effect of ALS-derived DEM uncertainty for quantifying changes due to the landslide in 2011, Mt. Umyeon, Seoul. *GISci Remote Sens* 57(3): 287–301
- Kyriou A, Nikolakopoulos K (2018) Assessing the suitability of Sentinel-1 data for landslide mapping. *Eur J Remote Sens* 51(1):402–411
- Lindner G, Schraml K, Mansberger R, Hübl J (2016) UAV monitoring and documentation of a large landslide. *Appl Geomat* 8(1):1–11
- Lucieer A, de Jong SM, Turner D (2014) Mapping landslide displacements using structure from motion (SfM) and image correlation of multi-temporal UAV photography. *Prog Phys Geogr* 38(1):97–116
- Martin-Duque JF, Sanz MA, Bodoque JM, Lucia A, Martin-Moreno C (2010) Restoring earth surface processes through landform design—a 13-year monitoring of a geomorphic reclamation model for quarries on slopes. *Earth Surf Proc Land* 35:531–548
- Mateos RM, Azañón JM, Roldán FJ, Notti D, Pérez-Peña V, Galve JP, Pérez-García JL, Colomo CM, Gómez-López JM, Montserrat O, Devantèry N, Lamas-Fernández F, Fernández-Chacón F (2017) The combined use of PSInSAR and UAV photogrammetry techniques for the analysis of the kinematics of a coastal landslide affecting an urban area (SE Spain). *Landslides* 14:743–754
- Matese A (2020) Editorial for the special issue "Forestry Applications of Unmanned Aerial Vehicles (UAVs)". *Forests* 11:406
- Mura JC, Paradella WR, Gama FF, Silva GG, Galo M, Camargo PO, Silva AQ, Silva A (2016) Monitoring of non-linear ground movement in an open pit iron mine based on an integration of advanced DInSAR techniques using TerraSAR-X data. *Remote Sens* 8(5):409
- Niethammer U, Rothmund S, Joswig M (2009) UAV-based remote sensing of the slow-moving landslide Super-Sauze J-P. In: Malet J-P, Remaître A, Boogard T (eds) *Proceedings of the international conference on landslide processes: from geomorphologic mapping to dynamic modelling*. CERG Editions, Strasbourg, pp 69–74
- Osmanoğlu B, Dixon TH, Wdowinski S, Cabral-Cano E, Jiang Y (2011) Mexico City subsidence observed with persistent scatterer InSAR. *Int J Appl Earth Obs Geoinf* 13:1–12
- Pasquali P, Cantone A, Riccardi P, Defilippi M, Ogushi F, Gagliano S, Tamura M (2014) Mapping of ground deformations with interferometric stacking techniques. In: Holecz F, Pasquali P, Milisavljevic N (eds) *Land applications of radar remote sensing*. Intech 234–259
- Peterman V (2015) Landslide activity monitoring with the help of unmanned aerial vehicle. *The International Archives of the Photogrammetry, Remote Sensing and Spatial Information Sciences* Volume XL-1/W4. In: 2015 international conference on unmanned aerial vehicles in geomatics, 30 Aug–02 Sept, Toronto, Canada, pp 215–218
- Peternal T, Kumelj S, Ostir K, Komac M (2017) Monitoring the Potoška planina landslide (NW Slovenia) using UAV photogrammetry and tachymetric measurements. *Landslides* 14:395–406
- Poyraz F, Gül Y, Duymaz B (2020) Determination of deformations by using the PSI technique at a common dump site of three different open-pit marble mines in Turkey. *Turkish J Earth Sci* 29:1004–1016
- Prati C, Ferretti A, Perissin D (2010) Recent advances on surface ground deformation measurement by means of repeated space-borne SAR observations. *J Geodyn* 49:161–170
- Prokešová R, Kardoš M, Medved'ová A (2010) Landslide dynamics from high-resolution aerial photographs: a case study from the Western Carpathians. *Slovakia Geomorphol* 115(1–2):90–101
- Razi P, Sri Sumantyo JT, Perissin D, Kuze H, Chua MY, Panggabean GF (2018) 3D land mapping and land deformation monitoring using persistent scatterer interferometry (PSI) ALOS PALSAR: validated by Geodetic GPS and UAV. *IEEE Access* 6:12395–12404
- Sarmap (2013) SBAS tutorial, available at https://www.sarmap.ch/tutorials/sbas_tutorial_V_2_0.pdf
- Sarmap (2014) PS Tutorial, available at http://www.sarmap.ch/tutorials/PS_Tutorial_V_0_9.pdf

- Silvia B, Francesca C, Chiara DV, Sandro M, Nicola C (2013) Monitoring landslide induced displacements with TerraSAR-X persistent scatterer interferometry (PSI): Gimigliano case study in Calabria Region (Italy). *Int J Geosci* 4:1467–1482
- Sonter LJ, Barrett DJ, Soares-Filho BS (2014) Offsetting the impacts of mining to achieve no net loss of native vegetation. *Conserv Biol* 28(4):1068–1076
- Strozzi T, Farina P, Corsini A, Ambrosi C, Thüring M, Zilger J et al (2005) Survey and monitoring of landslide displacements by means of L-band satellite SAR interferometry. *Landslides* 2:193–201
- Strozzi T, Ambrosi C, Raetz H (2013) Interpretation of aerial photographs and satellite SAR interferometry for the inventory of landslides. *Remote Sens* 5:2554–2570
- Tang W, Motagh M, Zhan W (2020) Monitoring active open-pit mine stability in the Rhenish coalfields of Germany using a coherence-based SBAS method. *Int J Appl Earth Obs Geoinf* 93:102217
- Tanteri L, Rossi G, Tofani V, Vannocci P, Moretti S, Casagli N (2017) Multitemporal UAV survey for mass movement detection and monitoring. In: Mikoš M et al. (eds) *Advancing culture of living with landslides*. Doi: https://doi.org/10.1007/978-3-319-53498-5_18
- Tarolli P (2014) High-resolution topography for understanding earth surface processes: opportunities and challenges. *Geomorphology* 216:295–312
- Turner D, Lucieer A, de Jong SM (2015) Time series analysis of landslide dynamics using an unmanned aerial vehicle (UAV). *Remote Sens* 7:1736–1757
- Ulusay R, Gökçeoğlu C, Sönmez H, Tuncay E (2001) Causes, mechanism and environmental impacts of instabilities at Himmetoğlu coal mine and possible remedial measures. *Environ Geol* 40(6):769–786
- Vrublová D, Kapica R, Jiráňková E, Struś A (2015) Documentation of landslides and inaccessible parts of a mine using an unmanned UAV system and methods of digital terrestrial photogrammetry. *GeoSci Eng* 61(3):8–19
- Wasowski J, Bovenga F (2014) Investigating landslides and unstable slopes with satellite Multi Temporal Interferometry: current issues and future perspectives. *Eng Geol* 174:103–138
- Wegmüller U, Walter D, Spreckels V, Werner C (2010) Nonuniform ground motion monitoring with TerraSAR-X persistent scatterer interferometry. *IEEE Trans Geosci Remote Sens* 48(2):895–904
- Yhokha A, Chang CP, Goswami PK, Yen JY, Lee SI (2015) Surface deformation in the Himalaya and adjoining piedmont zone of the Ganga Plain, Uttarakhand, India: Determined by different radar interferometric techniques. *J Asian Earth Sci* 106:119–129
- Zhang Y, Meng X, Jordan C, Novellino A, Dijkstra T, Chen G (2018) Investigating slow-moving landslides in the Zhouqu region of China using InSAR time series. *Landslides* 15:1200–1315
- Zhang L, Liao M, Balz T, Shi X, Jiang Y (2015) Monitoring landslide activities in the three Gorges area with multi-frequency satellite SAR data sets. In: Scaioni M (eds) *Modern technologies for landslide monitoring and prediction*. Springer Natural Hazards, Berlin
- Zhao C, Lu Z (2018) Remote sensing of landslides—a review. *Remote Sens* 10:279. <https://doi.org/10.3390/rs10020279>
- Zhao Q, Lin H, Jiang L, Chen F, Cheng S (2009) A study of ground deformation in the Guangzhou urban area with persistent scatterer interferometry. *Sensors* 9:503–518
- Zhao C, Lu Z, Shang Q, de la Fuente J (2012) Large-area landslide detection and monitoring with ALOS/PALSAR imagery data over Northern California and Southern Oregon, USA. *Remote Sens Environ* 124:348–359

Publisher's Note Springer Nature remains neutral with regard to jurisdictional claims in published maps and institutional affiliations.